Length scales, collective modes, and type-1.5 regimes in three-band superconductors

Johan Carlström,[1,2] Julien Garaud,[2] and Egor Babaev[1,2]
[1]*Department of Theoretical Physics, The Royal Institute of Technology, SE-10691 Stockholm, Sweden*
[2]*Department of Physics, University of Massachusetts, Amherst, Massachusetts 01003, USA*
(Received 23 July 2011; published 17 October 2011)

The recent discovery of iron pnictide superconductors has resulted in a rapidly growing interest in multiband models with more than two bands. In this work we specifically focus on the properties of three-band Ginzburg-Landau models which do not have direct counterparts in more studied two-band models. First we derive normal modes and characteristic length scales in the conventional $U(1)$ three-band Ginzburg-Landau model as well as in its time-reversal symmetry-broken counterpart with $U(1) \times Z_2$ symmetry. We show that, in the latter case, the normal modes are mixed phase-density collective excitations. A possibility of the appearance of a massless mode associated with fluctuations of the phase difference is also discussed. Next we show that gradients of densities and phase differences can be inextricably intertwined in vortex excitations in three-band models. This can lead to very long-range attractive intervortex interactions and the appearance of type-1.5 regimes even when the intercomponent Josephson coupling is large. In some cases it also results in the formation of a domainlike structure in the form of a ring of suppressed density around a vortex across which one of the phases shifts by π. We also show that field-induced vortices can lead to a change of broken symmetry from $U(1)$ to $U(1) \times Z_2$ in the system. In the type-1.5 regime, it results in a semi-Meissner state where the system has a macroscopic phase separation in domains with broken $U(1)$ and $U(1) \times Z_2$ symmetries.

DOI: 10.1103/PhysRevB.84.134518 PACS number(s): 74.70.Xa, 74.20.Mn, 74.20.Rp

I. INTRODUCTION

Superconductivity with two gaps associated with different bands was first theoretically predicted in 1959.[1,2] However, it was not until 42 years later, with the discovery of MgB_2 (Ref. 3), that it started to attract wide interest (for a recent review see Ref. 4). Because the condensates in two-band superconductors are not independently conserved, the system considered in Refs. 1 and 2 shares the same broken $U(1)$ symmetry of the ground state as their single-component counterparts. The interband tunneling results in a system that attains its free-energy minimum when the phase difference between the condensates is either zero or π. Nonetheless in 1969 it was discussed that individual phases of the two condensate wave functions are important degrees of freedom, since they give rise to a new kind of collective excitations. These collective excitations are associated with the fluctuations of the relative phase of the two superconducting components around its ground-state value: the Leggett mode[5] (for a recent discussion see Ref. 6). A report of the observation of the Leggett mode in MgB_2 appeared very recently.[7]

Another example of new physics which can arise in two-band systems (as compared to their single-band counterparts) is associated with a disparity of the characteristic length scales of density variations. That is, a single quantum vortex in a two-band system should in general produce two different cores. As a consequence of this, there appears a regime which was recently termed type-1.5 superconductivity.[8] In that regime the two characteristic length scales of density variations ξ_1 and ξ_2 satisfy the condition $\xi_1 < \sqrt{2}\lambda < \xi_2$. For a subset of parameters in this regime there are thermodynamically stable vortices with nonmonotonic interaction. Namely, these vortices exhibit interaction which is long-range attractive, and short-range repulsive. As a consequence of the long-range attraction between vortices, the system allows an additional "semi-Meissner" phase associated with macroscopic phase separations in domains of the Meissner state and vortex states (see, e.g., Refs. 8–15). For a detailed introduction see Ref. 16.

In the last 3 years there has been a rapidly growing interest in multiband superconductivity with more than two components. The interest was sparked by the recent discovery of iron pnictide superconductors[17] and subsequent discussions that superconductivity in these systems may be described by a theory with more than two relevant bands.[18,19] It was observed that the inclusion of a third band in the theory in several respects leads to qualitatively different physics compared to two-band systems.[20–23] The new physics arises from the fact that the presence of three or more components can lead to phase frustration. It results from competition of three or more interband Josephson coupling terms, which cannot all simultaneously attain the most energetically favorable phase-locking pattern.[20–23] This frustration leads to time-reversal symmetry breakdown (TRSB).[20–24] (We discuss it more quantitatively below.) See also Refs. 25 and 26 for a different discussion of possible time-reversal symmetry breakdown in iron pnictides. Here we show that phase frustration leads to a plethora of new phenomena in the physics of collective excitations and the magnetic response of the three-band Ginzburg-Landau model.

In the TRSB phase there are no "phase-only" Leggett modes. Instead there is a different kind of collective excitations: mixed phase-density modes. These mixed normal modes have quite complex structure, and they can possess modes with large characteristic length scales even in the case of strong Josephson coupling. At the transition point to the TRSB regime, the length scale of one of the phase-difference modes diverges, rendering one of the modes massless (as was also discussed recently in a London model;[27] for other recent discussions of Leggett's modes in connection with iron pnictides see Refs. 28 and 29). Note however that if the phase transition in TRSB state is first order as

was argued in Ref. 21, then there will no massless mode. This is in contrast to two-band systems where increasing interband Josephson coupling always diminishes disparities of the density variations.[10,16] In particular it implies that the type-1.5 regime is possible in three-band superconductors even in cases of quite strong interband Josephson coupling. Moreover we show that in three-band systems the semi-Meissner state can represent not only a macroscopic phase separation in vortex and Meissner domains but also a macroscopic phase separation of domains with different broken symmetries.

II. MODEL

The minimal Ginzburg-Landau (GL) free-energy functional to model a three-band superconductor is

$$F = \frac{1}{2}(\nabla \times \mathbf{A})^2 + \sum_{i=1,2,3} \frac{1}{2}|\mathbf{D}\psi_i|^2 + \alpha_i|\psi_i|^2 + \frac{1}{2}\beta_i|\psi_i|^4 + \sum_{i=1,2,3}\sum_{j>i} \eta_{ij}|\psi_i||\psi_j|\cos(\varphi_{ij}). \quad (1)$$

Here $\mathbf{D} = \nabla + ie\mathbf{A}$ and $\psi_i = |\psi_i|e^{i\varphi}$ are complex fields representing the superconducting components. The phase difference between two condensates is denoted $\varphi_{ij} = \varphi_j - \varphi_i$. The magnetic flux density through the system is given by $\mathbf{B} = (\nabla \times \mathbf{A})$ and the magnetic energy density is $\mathbf{B}^2/2$. Such a multicomponent GL free energy can in certain cases be microscopically derived at temperatures close but not too close to T_c (for a review see Ref. 30). Indeed the existence of three superconducting bands is not by any means a sufficient condition for a system to have GL expansion like that given in Eq. (1). However, many of the questions which we consider below in fact do not require the system to be in the high-temperature region where a GL expansion like Eq. (1) could in certain cases be formally justified. In what follows, however, we use the minimal GL model since it provides a convenient framework to discuss this physics qualitatively. In Eq. (1) the coefficients α_i change signs at some characteristic temperatures which are generally different for all components. Below this temperature, $\alpha_i < 0$ and the band is active. Above it, $\alpha_i > 0$ and the band is passive. Passive bands can nevertheless have nonzero superfluid density because of the interband Josephson tunneling terms $\eta_{ij}|\psi_i||\psi_j|\cos\varphi_{ij}$. Thus it is possible in this model to have only passive bands and still nonzero superfluid densities due to Josephson terms. In the three-component model of Eq. (1) there are additional terms allowed by symmetry, e.g., biquadratic terms in density. (For a review of microscopic derivation of such terms from a weak-coupling two-band theory see Ref. 30.) However, the impact of these terms on length scales and vortex physics in the three-band model is essentially the same as in the well-studied two-band case.[16] Since their role is mostly connected with a straightforward renormalization of the length scales, we do not repeat this analysis here. Instead we focus primarily on the Josephson couplings, which can play principally different roles in two- and three-band cases.

Let us first discuss the simplest London approximation, i.e., $|\psi| = \text{const}$. Then one can extract gradients of the gauge-invariant phase differences by rewriting the model as

$$F = \frac{1}{2\sum_{i=1,2,3}|\psi_i|^2}\left[\sum_{i=1,2,3}|\psi_i|^2\nabla\varphi_i + e\sum_{i=1,2,3}|\psi_i|^2\mathbf{A}\right]^2 + \frac{|\psi_1||\psi_2|}{4\sum_{i=1,2,3}|\psi_i|^2}[\nabla(\varphi_1-\varphi_2)]^2 + \frac{|\psi_2||\psi_3|}{4\sum_{i=1,2,3}|\psi_i|^2}[\nabla(\varphi_2-\varphi_3)]^2 + \frac{|\psi_1||\psi_3|}{4\sum_{i=1,2,3}|\psi_i|^2}[\nabla(\varphi_1-\varphi_3)]^2 + \sum_{i=1,2,3}\sum_{j>i}\eta_{ij}|\psi_i||\psi_j|\cos(\varphi_i-\varphi_j) + \frac{1}{2}(\nabla\times\mathbf{A})^2. \quad (2)$$

The first term features the phase gradients coupled to the vector potential: this corresponds to the total current in the system. The rest of the terms correspond to counterflow of carriers in different bands. Since there is no charge transfer in counterflows there is no coupling to gauge fields. In the limit $\eta_{ij} = 0$, the second, third, and fourth terms describe neutral superfluid modes with phase stiffnesses $|\psi_i||\psi_j|/[4\sum_{i=1,2,3}|\psi_i|^2]$ which were studied in detail in Ref. 31. When Josephson terms are present they break symmetry by giving preferred values to the phase differences, yet the system can have fluctuations near these values. After this illustration of phase fluctuations, we discuss in the following the fluctuations within the full Ginzburg-Landau model which involves fluctuations of both phases and densities.

Systems with more than two Josephson-coupled bands can exhibit *phase frustration*. For $\eta_{ij} < 0$, a given Josephson interaction energy term is minimal for zero phase difference (we then refer to the coupling as "phase locking"), whereas when $\eta_{ij} > 0$ it is minimal for a phase difference equal to π (we then refer to the coupling as "phase antilocking"). Two-component systems are symmetric with respect to the sign change $\eta_{ij} \to -\eta_{ij}$ as the phase difference changes by a factor π, for the system to recover the same interaction. However, in systems with more than two bands there is generally no such symmetry. For example, if a three-band system has $\eta > 0$ for all Josephson interactions, then these terms cannot be simultaneously minimized, as this would correspond to all possible phase differences being equal to π.

III. GROUND STATE OF A THREE-BAND SUPERCONDUCTOR

The ground-state values of the fields $|\psi_i|$ and φ_{ij} of system (1) are found by minimizing its potential energy,

$$\sum_i\left\{\alpha_i|\psi_i|^2 + \frac{1}{2}\beta_i|\psi_i|^4\right\} + \sum_{j>i}\eta_{ij}|\psi_i||\psi_j|\cos(\varphi_{ij}). \quad (3)$$

Minimizing potential energy equation (3) cannot in general be done analytically. Yet, some properties can be derived from qualitative arguments. In terms of the sign of the η's, there are four principal situations:

Case	Sign of $\eta_{12},\eta_{13},\eta_{23}$	Ground-state phases
1	$---$	$\varphi_1=\varphi_2=\varphi_3$
2	$--+$	Frustrated
3	$-++$	$\varphi_1=\varphi_2=\varphi_3+\pi$
4	$+++$	Frustrated

Case 2 can result in several ground states. If $|\eta_{23}| \ll |\eta_{12}|$, $|\eta_{13}|$, then the phase differences are generally $\varphi_{ij}=0$. If, on the other hand, $|\eta_{12}|$, $|\eta_{13}| \ll |\eta_{23}|$ then $\varphi_{23}=\pi$ and φ_{12} is either 0 or π. For certain parameter values it can also have compromise states with φ_{ij} not being integer multiples of π.

Case 4 can give a wide range of ground states, as can be seen in Fig. 1. As η_{12} is scaled, ground-state phases change continuously from $(-\pi, \pi, 0)$ to the limit where one band is depleted and the remaining phases are $(-\pi/2, \pi/2)$.

An important property of potential energy equation (3) is that it is invariant under complex conjugation of the fields. That is, the potential energy does not change if the sign of all phase differences is changed, $\varphi_{ij} \to -\varphi_{ij}$. Thus, if any of the phase differences φ_{ij} is not an integer multiple of π, then the ground state possesses an additional discrete Z_2 degeneracy. For example, for a system with $\alpha_i=-1$, $\beta_i=1$,

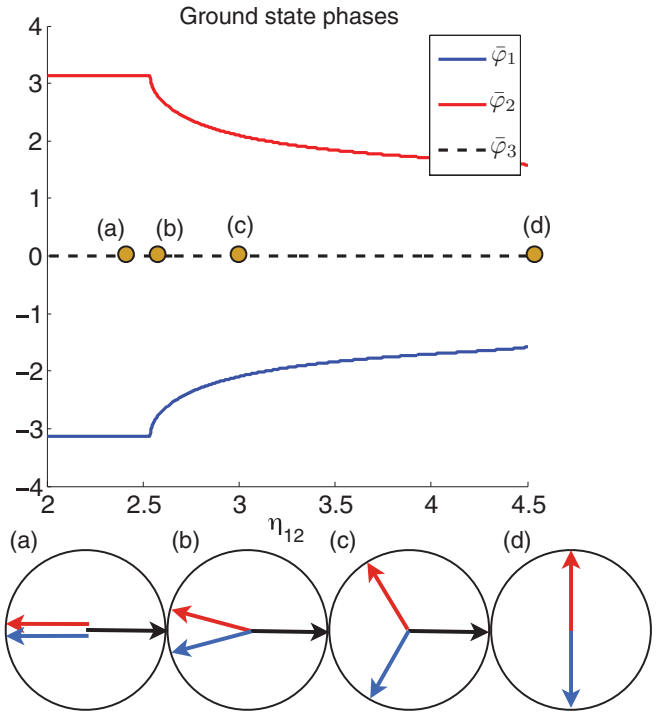

FIG. 1. (Color online) Ground-state phases of the three components as function of η_{12} (here $\varphi_3=0$ fixes the gauge). The GL parameters are $\alpha_i=1$, $\beta_i=1$, and $\eta_{13}=\eta_{23}=3$. For intermediate values of η_{12} the ground state exhibits discrete degeneracy [symmetry is $U(1)\times Z_2$ rather than $U(1)$] since the energy is invariant under the sign change $\varphi_2 \to -\varphi_2$, $\varphi_3 \to -\varphi_3$. For large η_{12} we get $\varphi_2-\varphi_3=\pi$, implying that $|\psi_3|=0$, and so there is a second transition from $U(1)\times Z_2$ to $U(1)$ and only two bands at the point (d). Here, the phases were computed in a system with only passive bands, though systems with active bands exhibit the same qualitative properties except for the transition to $U(1)$ and two bands only (i.e., active bands have nonzero density in the ground state).

and $\eta_{ij}=1$, two possible ground states are given by $\varphi_{12}=2\pi/3$, $\varphi_{13}=-2\pi/3$ or $\varphi_{12}=-2\pi/3$, $\varphi_{13}=2\pi/3$. Thus, in this case, the symmetry is $U(1)\times Z_2$, as opposed to $U(1)$. As a result, like any other system with Z_2 degeneracy, the theory allows an additional set of topological excitations: domain walls interpolating between the two inequivalent ground states. Under certain conditions the system also does allow composite topological excitations which are bound states of closed-domain walls and vortices.[32]

We are interested in determining quantitatively (i) the ground-state densities and phase differences and (ii) the characteristic length scales at which a perturbed field recovers its ground-state values. These quantities are derived from a perturbative expansion around the ground state. Consider the following expansion of the fields entering the Ginzburg-Landau free-energy functional Eq. (1), around the ground state:

$$\begin{aligned}\psi_i &= [u_i+\epsilon_i(r)]\exp\{i[\bar\varphi_i+\phi_i(r)]\},\\ \mathbf{A} &= \left(\frac{a(r)}{r}\right)(\sin\theta,\cos\theta).\end{aligned} \tag{4}$$

The ground-state densities and phases are denoted u_i and $\bar\varphi_i$, respectively. Since we are interested in vortex excitations, we consider an axially symmetric configuration by requiring that the field fluctuations $\epsilon_i(r)$, $\phi_i(r)$, and $a(r)$ depend only on the radial coordinate. The expansion equation (4) is inserted into the free energy equation (1) which is then sorted by growing orders in the fluctuations, namely $F=F^{(0)}+F^{(1)}+F^{(2)}+\cdots$. The condensation energy is given by $F^{(0)}$.

A. Ground state

The ground state can be represented by the vector of the zero-order degrees of freedom of Eq. (4),

$$\gamma^{(0)}=(u_1,u_2,u_3,\bar\varphi_1,\bar\varphi_2,\bar\varphi_3)^T. \tag{5}$$

The fluctuation amplitudes are collected in the six-entry vector

$$\gamma^{(1)}=(\epsilon_1,\epsilon_2,\epsilon_3,\phi_1,\phi_2,\phi_3)^T. \tag{6}$$

The gauge field fluctuation a decouples from the other fluctuations. The term in the GL free energy which is linear in the fluctuations reads

$$\begin{aligned}F^{(1)} = &\sum_i 2u_i\epsilon_i(\alpha_i+\beta_i u_i^2)+\sum_{j>i}\eta_{ij}(u_i\epsilon_j+u_j\epsilon_i)\cos\bar\varphi_{ij}\\ &+\sum_{j>i}\eta_{ij}u_iu_j(\phi_j-\phi_i)\sin\bar\varphi_{ij},\end{aligned} \tag{7}$$

where $\bar\varphi_{ij}$ denote phase differences of the ground state. Equation (7) is a linear (in the fluctuations) system of six equations. Since we consider fluctuations near the ground state it has to be zero for any arbitrary fluctuation. Indeed, by definition, no fluctuation can decrease the energy of the ground state. Positive definiteness implies that all the prefactors of the fluctuations are zero. Thus expanding Eq. (7) and collecting the prefactors of the fluctuation amplitudes gives the system of six equations which determine the ground-state vector $\gamma^{(0)}=(u_1,u_2,u_3,\bar\varphi_1,\bar\varphi_2,\bar\varphi_3)^T$. The system reads explicitly

$$0=\alpha_1u_1+\beta_1u_1^3+\frac{\eta_{12}}{2}u_2\cos\bar\varphi_{12}+\frac{\eta_{13}}{2}u_3\cos\bar\varphi_{13}, \tag{8a}$$

$$0=\alpha_2u_2+\beta_2u_2^3+\frac{\eta_{12}}{2}u_1\cos\bar\varphi_{12}+\frac{\eta_{23}}{2}u_3\cos\bar\varphi_{23}, \tag{8b}$$

$$0 = \alpha_3 u_3 + \beta_3 u_3^3 + \frac{\eta_{13}}{2} u_1 \cos\bar{\varphi}_{13} + \frac{\eta_{23}}{2} u_2 \cos\bar{\varphi}_{23}, \quad (8c)$$

$$0 = -\eta_{12} u_1 u_2 \sin\bar{\varphi}_{12} - \eta_{13} u_1 u_3 \sin\bar{\varphi}_{13}, \quad (8d)$$

$$0 = \eta_{12} u_1 u_2 \sin\bar{\varphi}_{12} - \eta_{23} u_2 u_3 \sin\bar{\varphi}_{23}, \quad (8e)$$

$$0 = \eta_{13} u_1 u_3 \sin\bar{\varphi}_{13} + \eta_{23} u_2 u_3 \sin\bar{\varphi}_{23}. \quad (8f)$$

Except under very specific conditions this cannot be solved analytically. In this paper we aim at the most general structure of the ground state, so no further assumptions are made and the problem is solved using numerical methods (we here used the Newton-Raphson algorithm). For numerical calculations of the ground-state values of the fields, it is convenient to fix the gauge by, for example, imposing $\bar{\varphi}_1 = 0$.

B. Length scales

Once the ground state $\gamma^{(0)}$ is known, relevant information about the physics of the system can be extracted from the quadratic order $F^{(2)}$ of the fluctuation expansion (note that this is equivalent to considering linearized GL equations). The fluctuations are described by a system of Klein-Gordon equations for the six condensate fluctuations (three densities plus three phases), supplemented by a Proca field equation which describes fluctuations of the gauge field. For studying the system it may be convenient to switch to a slightly different basis,

$$\gamma^{(1)} = (\epsilon_1,\epsilon_2,\epsilon_3,\pi_1,\pi_2,\pi_3)^T, \quad \text{where} \quad \phi_i \equiv \frac{\pi_i}{u_i}, \quad (9)$$

since in this basis, the (squared) mass matrix of the Klein-Gordon system is symmetric. The results are straightforwardly switched back to the basis ϕ. The total functional at this order reads

$$F^{(2)} = E_{\text{Klein-Gordon}} + E_{\text{Proca}}, \quad (10)$$

where

$$E_{\text{Klein-Gordon}} \equiv \frac{1}{2}(\gamma^{(1)\prime})^2 + \gamma^{(1)}\mathcal{M}^2\gamma^{(1)},$$
$$E_{\text{Proca}} \equiv \frac{1}{2}\left(\frac{a'}{r}\right)^2 + \frac{e^2}{2}\sum_i u_i^2 a. \quad (11)$$

Here the prime denotes differentiation with respect to the radial coordinate r. The (squared) mass matrix $\mathcal{M}^2$ of the Klein-Gordon system can easily be read from

$$\gamma^{(1)}\mathcal{M}^2\gamma^{(1)} = \sum_i \epsilon_i^2(\alpha_i + 3\beta_i u_i^2) + \sum_{j>i}\eta_{ij}\epsilon_i\epsilon_j\cos\bar{\varphi}_{ij} + \sum_{j>i}\eta_{ij}\left\{(u_i\epsilon_j + u_j\epsilon_i)\left(\frac{\pi_j}{u_j} - \frac{\pi_i}{u_i}\right)\sin\bar{\varphi}_{ij} - \frac{u_i u_j}{2}\left(\frac{\pi_j}{u_j} - \frac{\pi_i}{u_i}\right)^2\cos\bar{\varphi}_{ij}\right\}, \quad (12)$$

simply by identifying the prefactors of the perturbations and filling the corresponding entries in the mass matrix. Before discussing in detail this mass matrix, let us consider the Proca equation, for the mass of the gauge field. It is the easiest length scale to derive, since the Proca equation for the gauge field fluctuation Eq. (11) decouples from all others. The London penetration depth of the magnetic field λ is the inverse mass of the gauge field, namely

$$\lambda \equiv \frac{1}{m_{\text{Proca}}} = \frac{1}{e\sqrt{\sum_i u_i^2}}. \quad (13)$$

Length scales associated with condensate degrees of freedom are obtained in a more complicated way. Indeed they are given by the eigenvalue spectrum of a system of six coupled (static) Klein-Gordon equations, whose (squared) mass matrix $\mathcal{M}^2$ is derived from Eq. (12). It may be instructive to obtain this mass matrix explicitly. First of all, let us remark that fluctuations can be separated into two groups, the "density amplitude" $\vec{f} = (f_1, f_2, f_3)^T$ and the "normalized phase amplitudes" $\vec{\pi} = (\pi_1,\pi_2,\pi_3)^T$. This mass matrix is a real symmetric matrix, which is not diagonal and whose eigenvalues are the (squared) masses of the normal modes. The eigenspectrum of $\mathcal{M}^2$ defines the (squared) masses of the physical modes. The inverse of each of the masses gives the characteristic length scales of the theory. For example, in a single-component theory the inverse mass of the fluctuations of the modulus of the order parameter $|\psi|$ is the coherence length (up to a factor of $\sqrt{2}$). In a two-component theory the fluctuations in the phase difference (the Leggett mode) are characterized by a mass, the inverse of which sets the length scale at which a perturbed phase difference recovers its ground-state values. In two-component models the density modes are mixed: i.e., the characteristic length scales of the density fields are associated with the linear combinations of the fields.[10,14,16] Physically this means that disturbing one density field necessarily perturbs the other. It also implies that, say in a vortex, the long-range asymptotic behavior of both density fields is governed by the same exponent, corresponding to a mixed mode with the lowest mass.

We see that in the three-component case a new situation can arise where different collective modes are possible which are associated with mixed density and phase modes. In the basis $(\vec{f},\vec{\pi})$, the (squared) mass matrix can be written in terms of four submatrices

$$\gamma^{(1)}\mathcal{M}^2\gamma^{(1)} = (\vec{f},\vec{\pi})\begin{pmatrix} M_{ff} & M_{f\pi} \\ M_{\pi f} & M_{\pi\pi}\end{pmatrix}\begin{pmatrix}\vec{f}\\ \vec{\pi}\end{pmatrix}. \quad (14)$$

Where M_{ff} and $M_{\pi\pi}$ are the self-coupling of density and phase fluctuations, while $M_{f\pi}$ and $M_{\pi f}$ blocks control the mixing of density modes and phase modes.

$$M_{ff} = \begin{pmatrix} \alpha_1 + 3\beta_1 u_1^2 & \bar{\eta}_{12} & \bar{\eta}_{13} \\ \bar{\eta}_{12} & \alpha_2 + 3\beta_2 u_2^2 & \bar{\eta}_{23} \\ \bar{\eta}_{13} & \bar{\eta}_{23} & \alpha_3 + 3\beta_3 u_3^2 \end{pmatrix},$$
$$M_{\pi\pi} = \frac{-1}{2}\begin{pmatrix} 2\frac{u_2\bar{\eta}_{12}+u_3\bar{\eta}_{13}}{u_1} & -\bar{\eta}_{12} & -\bar{\eta}_{13} \\ \bar{\eta}_{12} & 2\frac{u_1\bar{\eta}_{12}+u_3\bar{\eta}_{23}}{u_2} & -\bar{\eta}_{23} \\ -\bar{\eta}_{13} & -\bar{\eta}_{23} & 2\frac{u_1\bar{\eta}_{13}+u_2\bar{\eta}_{23}}{u_3}\end{pmatrix},$$
$$M_{f\pi} = M_{\pi f}^T = \begin{pmatrix} -\frac{\hat{\eta}_{12}u_2+\hat{\eta}_{13}u_3}{u_1} & \hat{\eta}_{12} & \hat{\eta}_{13} \\ -\hat{\eta}_{12} & \frac{\hat{\eta}_{12}u_1-\hat{\eta}_{23}u_3}{u_2} & \hat{\eta}_{23} \\ -\hat{\eta}_{13} & -\hat{\eta}_{23} & \frac{\hat{\eta}_{13}u_1+\hat{\eta}_{23}u_2}{u_3}\end{pmatrix}, \quad (15)$$

where for more compact expression we introduce new notations $\bar{\eta}_{ij} = \frac{\eta_{ij}}{2}\cos\bar{\varphi}_{ij}$ and $\hat{\eta}_{ij} = \frac{\eta_{ij}}{2}\sin\bar{\varphi}_{ij}$. Finally in order to derive the length scales associated with the condensate fluctuations, one has to diagonalize the matrix $\mathcal{M}^2$. Its eigenspectrum is the set of six squared masses $\mathcal{M}_i^2$, whose corresponding lengths $\ell_i = 1/\mathcal{M}_i$ are the physical length scales of a three-band superconductor. In Appendix A we also show how these length scales are expressed in different units. There is a spontaneously broken $U(1)$ symmetry associated with the simultaneous equal changes of all phases. The mass of this mode is zero and the eigenvector associated with this $U(1)$ zero mode can easily be decoupled. Thus one can reduce the size of the system. However, we prefer not to decouple this mode from the mass spectrum, since it provides a measure of the error of the numerical resolution of masses of other modes. The corresponding degree of freedom is described by the first term in Eq. (2); it is a $U(1)$ Goldstone boson which, due to its coupling to the gauge field $\mathbf{A}$, yields a massive vector field with the mass m_{Proca} via the Anderson-Higgs mechanism.

Unfortunately the eigenbasis of $\mathcal{M}^2$ cannot be known analytically, in the general case. We calculate it numerically below.

C. Numerical results

Figure 2 shows the ground state, eigenspectrum, and eigenvectors of the (squared) mass matrix in a frustrated three-band superconductor as a function of the Josephson couplings. The coupling η_{12} is fixed, while the horizontal axis gives the coupling coefficients η_{13} and η_{23}. Each eigenvector is a linear combination of the degrees of freedom that make up a physical mode, for which variation length scale is given by the square root of the inverse of the corresponding eigenvalue in the eigenspectrum. The system crosses over from $U(1)$ to the $U(1) \times Z_2$ TRSB state at $\eta_{13} = \eta_{23} \approx -3.69$. In the $U(1)$ regime, the density modes are mixed. However, as can be seen from the eigenvectors, there is no mixing between density modes and the phase modes. Thus, perturbations of the densities and of the phases recover independently of each other. The fluctuations of the phase modes are the three-component generalization of the standard Leggett modes. In the $U(1) \times Z_2$ regime the situation is the opposite, and all eigenvectors are mixed in density and phase. This indicates that any perturbation of the densities creates a perturbation to the phases, and vice versa.

There is a point where a Leggett mode becomes massless, as was also pointed out recently in the phase-only model in Ref. 27. This occurs at the transition from $U(1)$ to $U(1) \times Z_2$ (note however that the transition between these states can be first order as discussed in Ref. 21). In Fig. 2(c), eigenvalue 5 does indeed go to zero, indicating that the mass vanishes. The corresponding eigenvector can be seen in Fig. 2(h). In the $U(1)$ regime it corresponds to perturbation of phases 1 and 2. The physical implication is that the recovery of a perturbation at this point is governed not by an exponential, but by a power law. It is only a point in the parameter space where this mass is zero. However, there is a finite area in the parameter space around that point where, although the mode is massive, the length scale associated with it is anomalously large as a consequence of the frustration between Josephson couplings.

IV. VORTEX MATTER IN THREE-BAND TYPE-1.5 SUPERCONDUCTORS

A. Topological defects in three-band Ginzburg-Landau model

Let us start by outlining the basic properties of the vortex excitations. In case of a $[U(1)]^3$ Ginzburg-Landau model (i.e., when $\eta_{ij} = 0$) there are three "elementary" vortex excitations associated with 2π winding in only one of the phases: $\oint_\sigma \nabla\varphi_i = 2\pi$, where σ is a closed path around a vortex core. Such a vortex carries a fraction of flux quantum, as can be seen from the following argument:[31,33] the supercurrent in the case when there is a phase winding in only one phase is

$$\mathbf{J}_i = \frac{ie}{2}[\psi_i^*\nabla\psi_i - \psi_i\nabla\psi_i^*] - e^2\sum_k |\psi_k|^2\mathbf{A}. \tag{16}$$

Expressing $\mathbf{A}$ via gradients and choosing the contour σ far from the vortex core gives the following equation for the magnetic flux:

$$\begin{aligned}\Phi_i = \oint_\sigma \mathbf{A}d\mathbf{l} &= \frac{u_i^2}{\sum_{k=1,2,3} u_k^2}\frac{1}{e}\oint_\sigma \nabla\phi_i \\ &= \frac{u_i^2}{\sum_{k=1,2,3} u_k^2}\Phi_0,\end{aligned} \tag{17}$$

where Φ_0 is a flux quantum. Such a fractional vortex in the $[U(1)]^3$ case has logarithmically divergent energy. Thus in the external field a bulk three-component superconductor should form "composite" integer flux vortices which have phase winding in all components: $\oint_\sigma \nabla\varphi_1 = 2\pi$, $\oint_\sigma \nabla\varphi_2 = 2\pi$, $\oint_\sigma \nabla\varphi_3 = 2\pi$. When Josephson coupling is nonzero, then the energy of a fractional vortex diverges linearly[33] and thus a single integer flux vortex in a bulk superconductor can be viewed as a strongly bound state of three cocentered fractional flux vortices. Note that such a bound state will in general have three different sizes of vortex cores. The characteristic length scales of the density recovery in the vortex cores are determined by the inverse masses of normal modes calculated above. Note also that the role of Josephson interaction on vortices is different in the presence of domain walls in three-band $U(1) \times Z_2$ superconductors. Immediately at the domain wall the Josephson terms have energetically unfavorable values of the phase differences. Thus, if a composite vortex is placed on such a domain wall, the Josephson interaction can force a splitting of this vortex into fractional flux vortices, because the splitting will allow to attain a more favorable configuration of the phase differences.[32]

B. Qualitative argument on the vortex states in frustrated three-band superconductors

The ground state of a phase-frustrated superconductor is in many cases nontrivial, with phase differences being compromises between the various interaction terms. Inserting vortices in such a system can shift the balance between different competing couplings, since vortices can in general have different effects on the different bands. In particular, since the core sizes of vortices are not generally the same in all bands, vortex matter will typically deplete some components more than others and thus can alter the preferred values of the phase difference. So the minimal potential

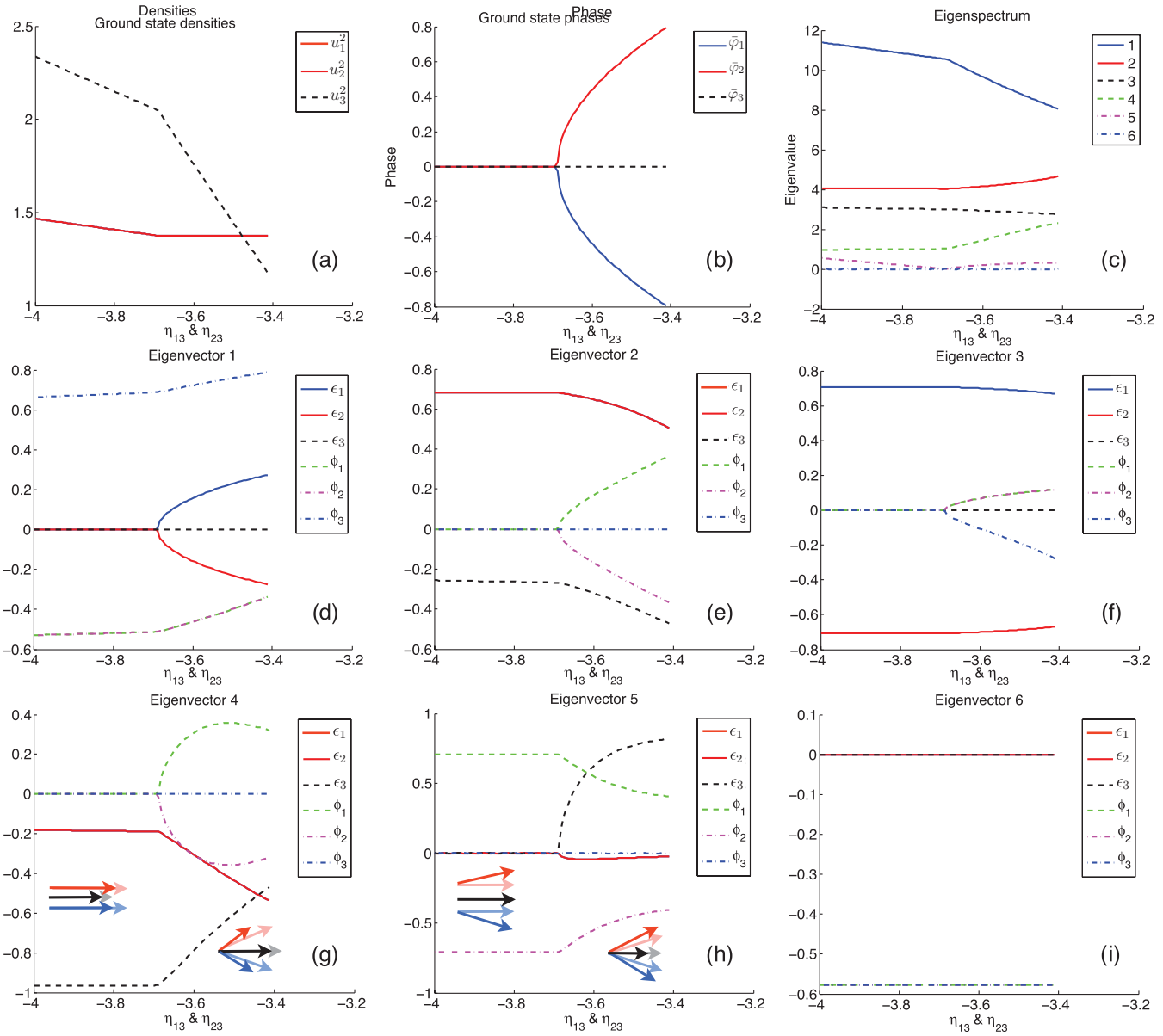

FIG. 2. (Color online) Ground state, eigenspectrum, and eigenvectors of the mass matrix. The x axis gives the two parameters $\eta_{13} = \eta_{23}$ while the other parameters are $\alpha_1 = -3$, $\beta_1 = 3$, $\alpha_2 = -3$, $\beta_2 = 3$, $\alpha_3 = 2$, $\beta_3 = 0.5$, and $\eta_{12} = 2.25$. The eigenvectors are sorted according to corresponding eigenvalue, starting with the largest. The smallest eigenvalue is the zero mode associated with the spontaneously broken $U(1)$ symmetry. At $\eta_{13} = \eta_{23} \approx -3.69$ there is a transition from $U(1)$ to $U(1) \times Z_2$. Eigenvalue 5 (c) becomes zero at the transition point, so there appears a divergent length scale at this point which corresponds to the eigenvector in (h); i.e., the phase difference mode becomes a scaleless collective excitation. Observe that, in the $U(1)$ region, the eigenvectors exhibit no mixing between densities and phases, whereas in the $U(1) \times Z_2$ region there is in fact not a single eigenvector that is not a mixing of phases and densities. Then, perturbations of densities are generically associated with perturbations of the phase differences in this regime. Arrows in (g) and (h) illustrate the variation of the fields associated with the corresponding collective modes. Length of the arrows corresponds to modulus fluctuation and the direction of the arrow corresponds to phase fluctuation. Order parameter of component 1 in red, component 2 in blue and component 3 in black.

energy inside a vortex lattice or cluster may correspond to a different set of phase differences than in the vortexless ground state. In this section we give a qualitative description of it, using an ansatz-based argument. In the following section we study this question numerically without involving an ansatz.

The qualitative argument is as follows. Consider the phase-dependent potential terms in the free-energy equation, Eq. (1), which are of the form

$$\eta_{ij} u_i u_j f_i(\mathbf{r}) f_j(\mathbf{r}) \cos\left(\varphi_{ij}(\mathbf{r})\right), \tag{18}$$

where u_i are ground-state amplitudes and each $f_i(\mathbf{r})$ represents an ansatz which models how superfluid densities are modulated due to vortices. Consider now a system where N vortices

are uniformly distributed in a domain Ω. The phase-dependent part of the free energy is

$$U_\varphi = \left[\sum_{i>j} \eta_{ij} u_i u_j\right] \int_\Omega d\mathbf{r}\, f_i(\mathbf{r}) f_j(\mathbf{r}) \cos(\varphi_{ij}(\mathbf{r})). \quad (19)$$

If φ_{ij} is varying slowly in comparison with the intervortex distance, then it can be considered constant in a uniform distribution of vortices (as a first approximation). In that case Eq. (19) can be approximated by

$$U_\varphi \simeq \sum_{ij} \tilde{\eta}_{ij} u_i u_j \cos(\varphi_{ij}), \text{ where } \tilde{\eta}_{ij} = \eta_{ij} \int_\Omega d\mathbf{r}\, f_i(\mathbf{r}) f_j(\mathbf{r}). \quad (20)$$

If, on the other hand, φ_{ij} varies rapidly, then it is not possible to define $\tilde{\eta}_{ij}$ without a spatial dependence. Then φ_{ij} will depend on $\tilde{\eta}_{ij}(\mathbf{r})$, which is related to the local modulation functions $f_i f_j$ and varies with a length scale given by the mass matrix Eq. (12).

Thus, $\tilde{\eta}$ is the effective interband interaction coupling resulting from density modulation. Since, in general, $f_i \neq f_j$ (unless the two bands i, j are identical), one must take into account the modulation functions f_i when calculating the phase differences. In particular, if the core size in component i is larger than in component j, then $\int d\mathbf{r}\, f_i f_k < \int d\mathbf{r}\, f_j f_k$ and therefore the phase differences φ_{ij} minimizing Eq. (20) depend on f_i and, consequently, on the density of vortices. Roughly speaking, introducing vortices in the system is equivalent to a relative effective decrease of some of the Josephson coupling constants.

Because the problem is nonlinear, the modulation functions f_i generally depend on φ_{ij} since the vortex core shape depends on the interband interactions. As a result, an exact solution to this problem can only be found by numerical methods. Below we address this problem by finding numerically vortex cluster solutions. Some qualitative statements can nonetheless be made about these systems:

(i) If band i is associated with larger vortex cores than band j, then, with increasing density of vortices, the effective Josephson coupling $\tilde{\eta}_{ik}$ is depleted faster than $\tilde{\eta}_{jk}$.

(ii) The average intercomponent phase difference in a vortex cluster depends on the parameters $\tilde{\eta}_{ij}$. So the intercomponent phase differences inside a vortex cluster can be different from the vortexless ground state. Superconductors with $U(1) \times Z_2$ symmetry and disparity of core sizes will therefore generally exhibit perturbation of the phase differences due to vortices.

(iii) The symmetry of the system depends on the interband interactions, so vortex matter can induce a phase transition between $U(1)$ and $U(1) \times Z_2$ states or vice versa.

This physics depends on the spatial distribution of vortices in the system.

If vortices are uniformly distributed in the sample, as is generally the case in clean type-2 superconductors, then the effective interband interaction strengths $\tilde{\eta}_{ij}$ are depleted in the same way everywhere in the sample. A change in broken symmetry $U(1) \to U(1) \times Z_2$ would then occur in the whole system at a certain value of applied external field.

It also opens a possibility of a type-1.5 regime qualitatively different in three-band systems than in their two-band counterparts. Indeed, because of the nonmonotonic interactions, the superconductor possesses macroscopic separation of Meissner domains and vortex clusters. In the three-band case, these phases can exhibit different broken symmetries, for example, Meissner domains with the $U(1)$ symmetry and vortex clusters having a different symmetry, $U(1) \times Z_2$. The $U(1) \times Z_2$ broken symmetry arises here because of the renormalization by vortices of the effective coupling constants $\tilde{\eta}_{ij}$. If there is a symmetry change $U(1) \to U(1) \times Z_2$ associated with vortex clusters in the system then there will be two kinds of vortex clusters corresponding to Z_2 states. They will coexist with the Meissner state voids which do not have the broken Z_2 symmetry. Clearly, because of this additional discrete symmetry, intercluster interaction should generally be affected by whether the clusters are in the same or in different Z_2 states. When the magnetic field increases, vortex clusters will merge and the entire system will be in the state with broken $U(1) \to U(1) \times Z_2$ symmetry.

C. Numerical results

We used numerical computations to examine the questions which were raised about vortex matter in the previous sections. The free-energy functional in Eq. (1) is minimized in the presence of vortex matter. In these simulations the variational problem was defined using a finite-element formulation provided by the FREEFEM++[34] library framework, using a nonlinear conjugate gradient method. Readers interested in more technical details can refer to Appendix B. From these numerical data, several observations about vortex matter in three-band systems can be made.

1. Vortex clusters with broken Z_2 symmetry

We have simulated vortex clusters in a type-1.5 regime in the system given in Fig. 2 for $\eta_{13} = \eta_{23} = -3.7$, i.e., in the $U(1)$ region but close to the transition to broken time-reversal symmetry. Thus, if the vortex core size in component 3 is larger than in bands 1 and 2, then we should expect the breakdown of time-reversal symmetry for a sufficiently high density of vortices. Figure 3 shows that this is indeed the case. In the ground state, all phases are equal ($\bar{\varphi}_1 = \bar{\varphi}_2 = \bar{\varphi}_3$), but, once vortex clusters are present, these phases are no longer preferable and two other equivalent phase-locking states develop. As the density of the third band is depleted, phase differences come to be increasingly dominated by the interband coupling between the two other bands. This coupling term is not minimal for $\varphi_1 = \varphi_2$.

2. Long-range intervortex forces

Vortex matter in this system is associated with substantial variations of the intercomponent phase differences. As discussed above, in the three-band system there is a phase-difference mode that becomes and less and less massive as we approach the transition to a TRSB state. Thus, in the vicinity of this point the mass of the corresponding mode can be very small and then characteristic lengths of its variation very large.

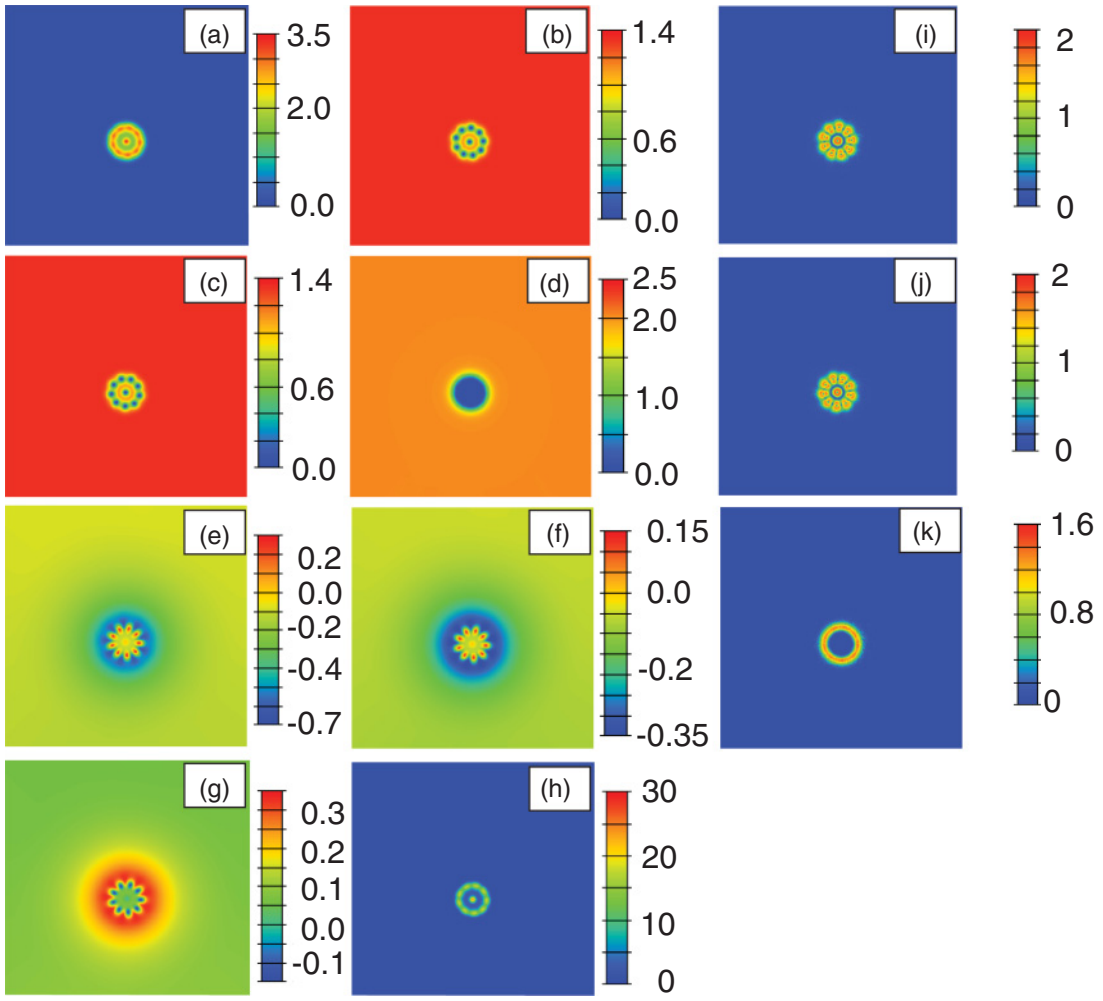

FIG. 3. (Color online) Vortex cluster exhibiting an internal Z_2 state in a frustrated three-band superconductor, showing (a) the magnetic field, and the densities of the different condensates are (b) $|\psi_1|^2$, (c) $|\psi_2|^2$, and (d) $|\psi_3|^2$. To monitor the relative phase differences, we use (e) $|\psi_1||\psi_2|\sin(\varphi_{12})$, (f) $|\psi_1||\psi_3|\sin(\varphi_{13})$, and (g) $|\psi_2||\psi_3|\sin(\varphi_{23})$. (h) The energy density and the supercurrents in each condensate, (i) J_1, (j) J_2, and (k) J_3, are shown. The GL parameters used for this simulation are $\alpha_1 = -3$, $\beta_1 = 3$, $\alpha_2 = -3$, $\beta_2 = 3$, $\alpha_3 = 2$, $\beta_3 = 0.5$, $\eta_{12} = 2.25$, $\eta_{13} = -3.7$, $\eta_{23} = -3.7$. Thus, they correspond to the $U(1)$ region in Fig. 2, but close to the transition point to $U(1) \times Z_2$ symmetry. In the ground state, all the phases are locked ($\bar{\varphi}_1 = \bar{\varphi}_2 = \bar{\varphi}_3$) as a consequence of the Josephson couplings $\eta_{12} = \eta_{13} = -3.7$ dominating the interaction. Inside the vortex cluster the third condensate is depleted, so the coupling terms $\eta_{i3}|\psi_i||\psi_3|\cos(\varphi_{i3})$, $\{i = 1,2\}$, become much weaker while the term $|\psi_1||\psi_2|\eta_{12}\cos(\varphi_{12})$ becomes dominant. In sufficiently dense vortex matter, the ground state is changed due to the dominating antilocking interaction between components 1 and 2. This results in a $U(1) \times Z_2$ state inside the vortex cluster, as can be seen from the phase-difference plots (e–g). (Note that in the very center of the vortex cluster this quantity is small because of small values of the prefactors $|\psi_i||\psi_j|$.) A closer inspection of (b) and (c) reveals that vortex cores in both densities do not necessarily superimpose [which can also be seen from the supercurrents in (i) and (j)] and so they are fractional vortices. This fractionalization occurs at the boundary of the cluster, while the vortex in the middle is a composite one-quantum vortex.

This provides an additional mechanism that can lead to vortex interactions at very large distances. Figure 4 displays the same system as in Fig. 3, but with two vortex clusters rather than one. A clearly visible perturbation of the phase differences extends from the clusters well outside the region with magnetic field and far beyond the area with significant density suppression, providing a mechanism for long-range intercluster interaction.

3. *Vortex fractionalization in clusters*

Figures 3 and 4 also exhibit flux fractionalization. As previously mentioned, the model in Eq. (1) allows fractional vortex solutions, where only one of the phases φ_i winds 2π around some point while the rest do not. The flux carried by a single fractional vortex is given by Eq. (17). Two forces hold fractional vortices together as a one-quantum composite vortex in the three-component model. First is the interaction with the gauge field, which gives logarithmic interaction at long range.[31,33] The second is the Josephson coupling, which is asymptotically linear. In nonfrustrated superconductors the Josephson coupling gives attractive interaction between fractional vortices, but in frustrated systems this interaction can be repulsive, resulting in fractionalization of vortices.[32]

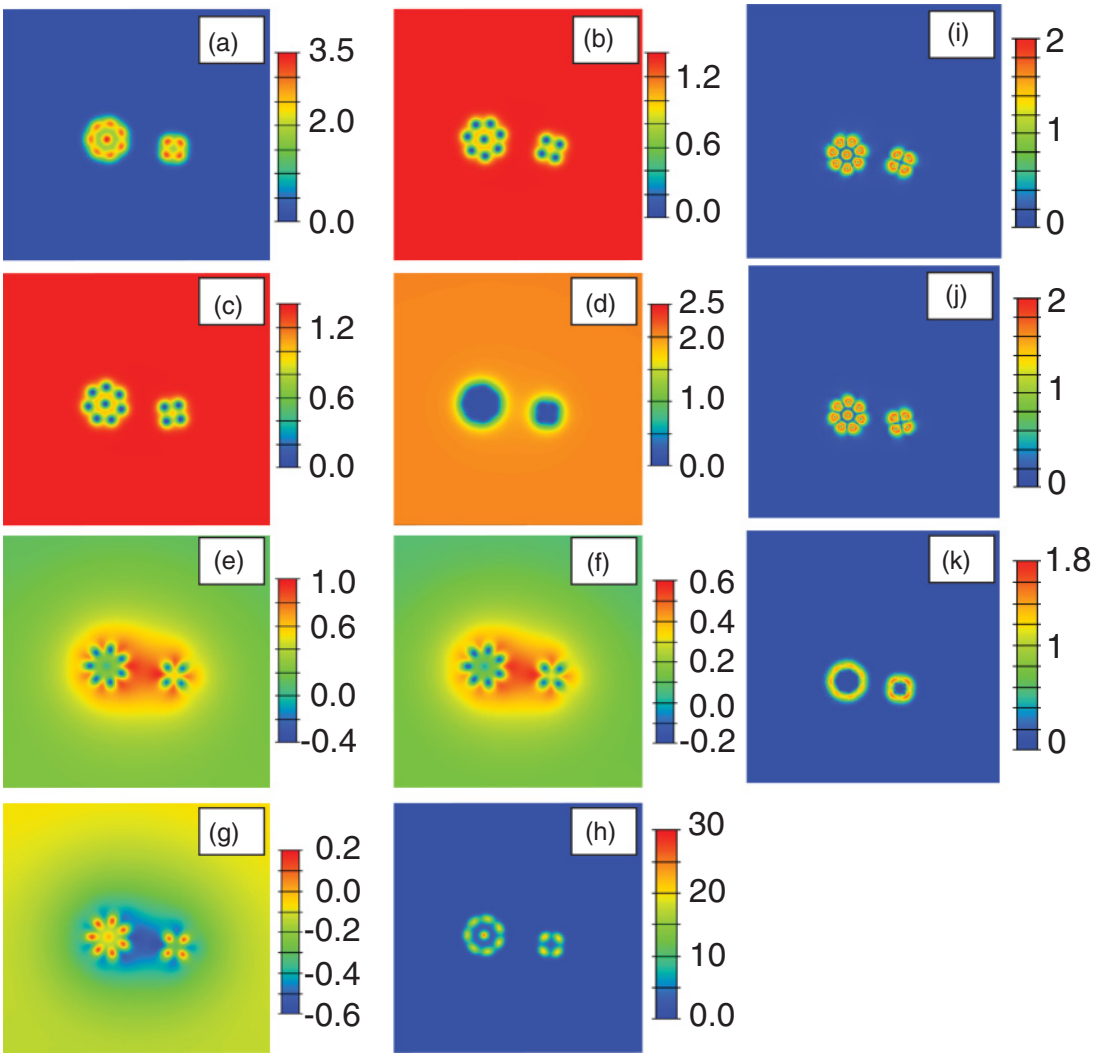

FIG. 4. (Color online) Interacting vortex clusters with internal Z_2 symmetry in a frustrated superconductor. The figure represents a state where the energy is well minimized with respect to all variables except the relative positions of the weakly interacting well-separated clusters. The GL parameters and displayed quantities and panel labels are the same as in Fig. 3. The analysis of the eigenvalues in Fig. 2 shows that there is a mode with a very small mass, associated with the eigenvector $[0,0,0,1,-1,0]$. It corresponds to the mode associated with phase-difference fluctuations and it has the largest recovery length scale. This is indeed visible in (e–g). The phase difference φ_{12} (e) recovers much more slowly than the magnetic field (a) and the condensate densities (b–d). Clusters clearly interact at a distance greatly exceeding the length scales of density modulation and the magnetic penetration depth, as this mode stretches out between them.

Consider the system in Figs. 3 and 4. The ground state corresponds to $\bar{\varphi}_1 = \bar{\varphi}_2 = \bar{\varphi}_3$. Since there is an energy cost associated with gradients of the phase difference, these are expected to change slowly. Thus, far away from the cluster, the state is simply the ground state. Deep inside the cluster, phase differences attain a broken $U(1) \times Z_2$ state, depending on the density of the vortex matter. If the vortex density is very high, then $|\psi_3|$ is very small, and we expect inside the cluster $\varphi_{12} \to \pi$ (provided that the cluster is large). While φ_{12} varies slowly, the density in $|\psi_3|$ recovers more rapidly at the boundary of the cluster. Thus, there may be an area where $|\varphi_{12}| < \pi/2$ while $|\psi_3|$ is small. Consequently the interaction between fractional vortices in bands 1 and 2 due to Josephson coupling is repulsive in this area. Also when the magnitude $|\psi_3|$ is very small or zero, the Josephson interband coupling ψ_{23} and ψ_{13} which provides attractive interaction between the fractional vortices is weaker or essentially disappears. Thus, the interaction of the fractional vortices is governed by the coupling to the gauge field, which gives attractive interaction, and the remaining Josephson coupling, which in this case gives repulsive interaction. As a result, in that region the integer flux vortices split into fractional ones.

This effect is found in numerical simulations of vortex clusters. Looking carefully at Figs. 3 and 4 we can see that the vortex cores in bands 1 and 2 do not generally coincide. From Figs. 3(g) and 4(g) we can read that, at the boundary of the cluster, the phase difference between components 1 and 2 is given by $|\psi_1||\psi_2| \sin(\varphi_{12}) \approx -0.7 \to |\varphi_{12}| \approx 0.5 \to \cos(\varphi_{12}) \approx \sqrt{3}/2 > 0$. Thus, in that region, the Josephson term associated with components 1 and 2 gives a positive energy contribution resulting in repulsive interaction between fractional vortices in components 1 and 2 leading to the

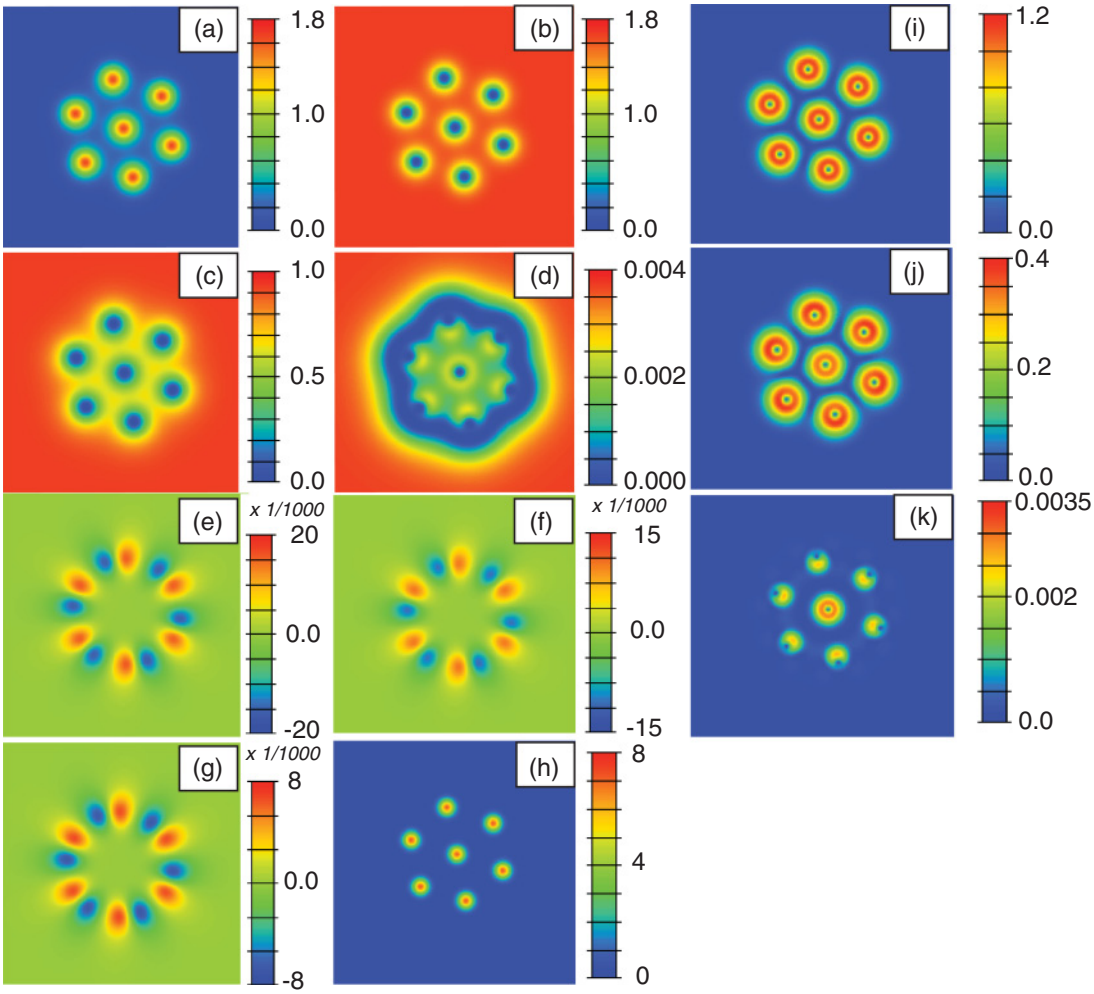

FIG. 5. (Color online) A vortex cluster surrounded by a π wall. Here again displayed quantities and panel labels are the same as in Fig. 3. The GL parameters are $\alpha_1 = -1$, $\beta_1 = 1$, $\alpha_2 = 1$, $\beta_2 = 0.5$, $\alpha_3 = 3$, $\beta_3 = 0.5$, $\eta_{12} = -2$, $\eta_{13} = 2.7$, and $\eta_{23} = -4$. In the ground state, the phases are locked ($\bar{\varphi}_1 = \bar{\varphi}_2 = \bar{\varphi}_3$), but frustration occurs as $\eta_{13} = 2.7$ gives an antilocking interaction (i.e., the term $|\psi_1||\psi_3|\eta_{13}\cos(\varphi_{13})$ is minimal for $\varphi_{13} = \pi$). As vortices are introduced in the system, the superfluid densities are depleted. It is clear from visual inspection that the vortices in the second band are larger than those of the first. Thus, the effective coupling $\tilde{\eta}_{23}$ decreases faster than $\tilde{\eta}_{13}$ and so inside the vortex cluster the preferred phase becomes $\varphi_1 = \varphi_2 = \varphi_3 + \pi$. Since the third band has much smaller density than the other bands, the energetically cheapest way of coping with this is to create a domain-wall-like object where $|\psi_3|$ becomes very small. It does not cost much energy to have a large phase gradient density, so that ψ_3 quickly picks up a π shift in its phase. As a result the density of $|\psi_3|$ is suppressed not only in the vortex cores but also in a ring surrounding the vortex cluster as can be clearly seen in (d).

fractionalization of vortices. Indeed, fractionalization occurs for all vortices except those in the center of the large eight- or nine-quanta clusters. We observe in large systems that fractionalization is important at the boundary of the clusters and becomes less pronounced for vortices located deep inside. The magnetic field is significantly smeared out as a result of this fractionalization.

The fractionalization at the cluster's boundary has a similar origin as the physics which stabilizes topological solitons in the TRSB states in three-band superconductors.[32] The difference is however that the topological solitons discussed in Ref. 32 are stable bound states of Z_2 domain walls and fractional vortices, while here there is not a Z_2 domain wall, but fractionalization comes as a result of complicated behavior of the fields at a cluster boundary which is an interface between $U(1)$ and $U(1) \times Z_2$ states.

4. π walls

Another phenomenon associated with frustrated superconductors are objects which we term "π walls." In certain parameter regions, vortices and vortex clusters are surrounded by a domain-wall-like object with substantially suppressed density, across which the phase of one of the condensates jumps by π.

An example of such an object is displayed in Fig. 5. The density in the third band is small in comparison to the other bands. The Josephson coupling $\eta_{12} = -2$ results in locked phases $\varphi_{12} = 0$. The system is frustrated, since $\eta_{23} = -4$, preferring phase locking with respect to φ_{23}, and $\eta_{13} = 2.7$, preferring phase antilocking with respect to φ_{13}. When there are no vortices in the system, the term $|\psi_2||\psi_3|\eta_{23}\cos\varphi_{23}$ dominates over $|\psi_1||\psi_3|\eta_{13}\cos\varphi_{13}$, and the ground state is $\bar{\varphi}_1 = \bar{\varphi}_2 = \bar{\varphi}_3$. However, when vortices are present in the

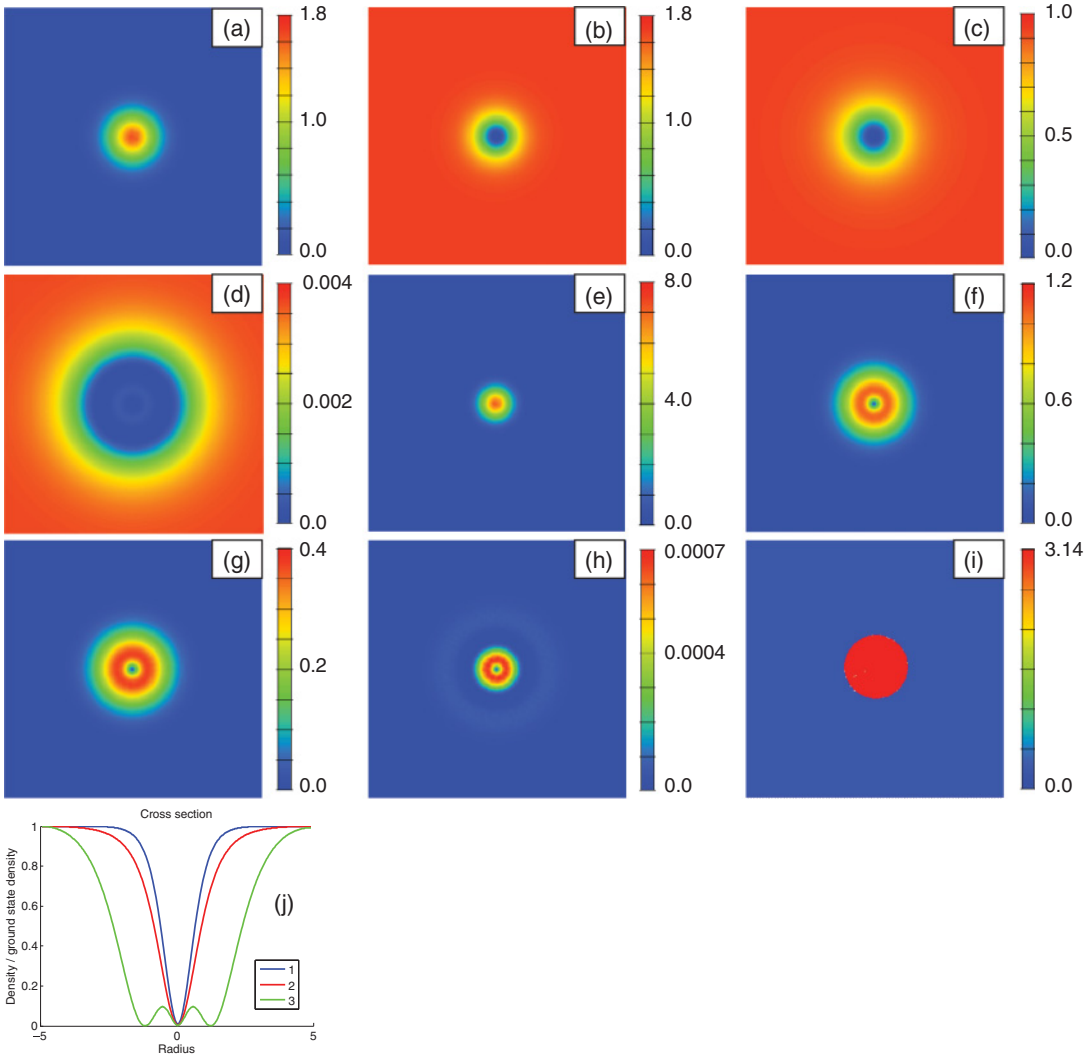

FIG. 6. (Color online) A single vortex in a system exhibiting π-wall solutions. The interband coupling coefficients are $\eta_{12} = -2$, $\eta_{13} = 2.7$, and $\eta_{23} = -4$. Displayed quantities here are (a) the magnetic flux and densities of each condensate (b) $|\psi_1|^2$, (c) $|\psi_2|^2$, and (d) $|\psi_3|^2$; (e) total energy density and supercurrents (f) J_1, (g) J_2, and (h) J_3; and (i) phase difference φ_{13}. The parameters of the system are identical to those given in Fig. 5. The π wall can be seen from the double dip in density of the third band as can be seen in (j), as well as from the phase difference plotted in (i). Thus, ψ_3 is zero in the center, it recovers slightly, and then it drops again on a circular area at a certain distance from the vortex center. At the second drop, the phase φ_3 picks up an extra phase π, as can be seen from the plot of φ_{13} in (i).

system, this is not necessarily the case. The vortex cores in the second band are larger than those of the first and, consequently, the effective coupling strength $\tilde{\eta}_{23}$ is diminished at a higher pace than $\tilde{\eta}_{13}$. Thus, inside a vortex cluster, the potential energy is minimal when $\varphi_{13} = \varphi_{23} = \pi$. To comply with these requirements, the system forms a domain-wall-like object where $|\psi_3|$ drops, and φ picks up an extra phase of π. For this particular set of parameters, this in fact happens even for a single vortex, as can be seen in Fig. 6.

V. CONCLUSIONS

Recently there has been a growing interest in three-band superconductivity sparked by the discovery of the iron pnictide superconductors. The precise information about the characteristic parameters for these materials is not known yet. Also the current experiments suggest that the physics of vortex ordering patterns in currently available samples is substantially affected by strong pinning.[35–40] We presented here a general study showing that in a three-band system there are many phenomena which are not present in two-band models. As was previously observed,[20–24,27] in the presence of more than two bands, a system can exhibit frustration between different competing interband Josephson terms. We considered possible physical consequences using a three-band Ginzburg-Landau model. To observe this physics in experiment in fact does not necessarily require a three-band superconductor but it would be sufficient to have a superconductor with phase-antilocking Josephson interaction (i.e., $\eta > 0$). Then, as was observed in Refs. 20 and 21, a phase-frustrated state can be induced in a Josephson-coupled bilayer made of this and single-band superconductors. The case of the Josephson couplings is just

real-space interlayer coupling. Thus, it provides an opportunity to tune its value.

We discussed that this can result in the appearance of modes with very long characteristic length scales even when the interband Josephson coupling is strong. Here we also discussed that in the TRSB $U(1) \times Z_2$ state of the three-band Ginzburg-Landau model there are no "phase-only" Leggett modes, but instead the system has different mixed phase-density collective modes which involve both phase and density fluctuations. The physics of the coupled modes and associated different length scales substantially affects vortex matter in the system. The vortices can interact at distances much larger than the length scale of magnetic field localization or the length scale at which most of the condensate density is recovered, because of the existence of slowly varying phase difference and low-mass mixed density modes. This can give rise to nonmonotonic intervortex interaction and type-1.5 regimes in systems where it would not be expected. In particular, if a large-κ parameter is estimated from the second critical field of the system, then this does not prohibit the existence of modes with length scales that substantially exceed the penetration depth even at strong Josephson coupling.

Moreover, the competing interactions can qualitatively affect the vortex structure as well. We showed the existence of a vortex solution where density not only is suppressed in the core but also takes a second dip in some beltlike area around the vortex core or around the vortex cluster. Such features can in principle be detected in scanning tunneling microscopy measurements.

Furthermore, we showed that subjecting a three-band system to an external field which induces vortices can shift the balance in competing interactions and result in change of the ground-state symmetry. In type-2 systems where vortices are uniformly distributed, changes in the phase difference will also occur quite uniformly; there could be a phase transition between $U(1)$ and $U(1) \times Z_2$ states resulting from an applied magnetic field. In the case of type-1.5 superconductivity, systems will feature not only macroscopic phase separation between vortex clusters and domains of Meissner state but also a macroscopic phase separation between the domains of $U(1)$ and $U(1) \times Z_2$ ground states. The transition from the semi-Meissner to vortex states in that case will then be associated with change of the symmetry from $U(1)$ to $U(1) \times Z_2$.

ACKNOWLEDGMENTS

This work is supported by the Swedish Research Council and by the Knut and Alice Wallenberg Foundation through the Royal Swedish Academy of Sciences fellowship and by NSF CAREER Award No. DMR-0955902.

APPENDIX A: UNIT SYSTEM

The Ginzburg-Landau free energy equation, Eq. (1), is written after suitable rescaling. Below we give details of these rescalings in order to define the various quantities in the usual dimensionful theory. In the following, let us denote the usual dimensionful quantities with a hacek over the variable. Consider the following:

$$\begin{aligned} \check{F} &= \frac{\hbar^2 c^2}{4\pi} F, \quad \check{\psi}_i = \sqrt{\frac{\check{m}c^2}{4\pi}}\psi_i, \quad \check{\mathbf{A}} = -\hbar c \mathbf{A}, \\ \check{\alpha}_i &= \frac{\hbar^2}{\check{m}}\alpha_i, \quad \check{\beta}_i = \frac{4\pi\hbar^2}{\check{m}^2 c^2}\beta_i, \quad \check{\eta}_{ij} = \frac{\hbar^2}{\check{m}}\eta_{ij}, \end{aligned} \tag{A1}$$

where c is the speed of light and $\hbar$ is the reduced Planck constant; then we convert the free-energy equation, Eq. (1), to

$$\begin{aligned} \check{F} = {} & \frac{1}{8\pi}(\nabla \times \check{\mathbf{A}})^2 + \sum_{i=1,2,3} \frac{\hbar^2}{2\check{m}} |\check{\mathbf{D}}\check{\psi}_i|^2 \\ & + \sum_{i=1,2,3} \check{\alpha}_i |\check{\psi}_i|^2 + \frac{1}{2}\check{\beta}_i |\check{\psi}_i|^4 \\ & + \sum_{i=1,2,3} \sum_{j>i} \check{\eta}_{ij} |\check{\psi}_i||\check{\psi}_j| \cos(\varphi_{ij}). \end{aligned} \tag{A2}$$

Here $\check{\mathbf{D}} = \nabla - i\frac{e}{\hbar c}\check{\mathbf{A}}$ and $\check{m}$ is the mass of the Cooper pairs.

This rescaling is also applied to the perturbative expansion of the problem, Eq. (4), so that the Klein-Gordon system becomes

$$\check{E}_{\text{Klein-Gordon}} \equiv \frac{\hbar^2}{2\check{m}}(\check{\gamma}^{(1)\prime})^2 + \check{\gamma}^{(1)}\mathcal{M}^2\check{\gamma}^{(1)}, \tag{A3}$$

and then, (dimensionful) length scales of the massive modes of the condensate are

$$\check{\xi}_i = \sqrt{\frac{2\hbar^2}{\check{m}}}\frac{1}{\mathcal{M}_i}. \tag{A4}$$

In the $U(1) \times Z_2$ regime, since all the modes are mixed, the length scales ξ_i then are related to inverse masses of the modes.

London penetration depth is defined through the Proca equation of the gauge field, which reads now in the dimensionful system as

$$\check{E}_{\text{Proca}} \equiv \frac{1}{8\pi}\left(\frac{\check{a}'}{r}\right)^2 + \frac{e^2\sum_i \check{u}_i^2}{2\check{m}c^2}\check{a}. \tag{A5}$$

London penetration depth, which gives the exponential decrement of the magnetic field in the superconductor, then reads

$$\check{\lambda}^2 = \frac{\check{m}c^2}{4\pi e^2 \sum \check{u}_i^2}. \tag{A6}$$

APPENDIX B: NUMERICAL METHODS: FINITE-ELEMENT ENERGY MINIMIZATION

We provide here a detailed description of the numerical methods which are used to construct vortex solutions in three-component Ginzburg-Landau models. They are constructed by minimizing the free-energy equation, Eq. (1), from an appropriate initial guess carrying several flux quanta. We consider the two-dimensional problem $\mathcal{F} = \int_\Omega F dx^2$ defined on the bounded domain $\Omega \subset \mathbb{R}^2$, supplemented by an "open" boundary conditions on $\partial\Omega$. This "open constraint" is a particular Neumann boundary condition such that the normal derivative of the fields on the boundary is zero. These boundary conditions in fact are a very weak constraint.

For this problem one could also apply Robin boundary conditions on $\partial\Omega$, so that the fields satisfy the linear asymptotic behavior (exponential localization) in Eq. (11). However, we choose to apply the open boundary conditions which are less constraining for the problem in question. Open boundary conditions also imply that vortices can easily escape from the numerical grid, since it would further minimize the energy. To prevent this, the numerical grid is chosen to be large enough so that the attractive interaction with the boundaries is negligible. The size of the domain is then much larger than the typical interaction length scales. Thus, in this method one has to use large numerical grids, which is computationally demanding. At the same time the advantage is that it is guaranteed that obtained solutions are not boundary pressure artifacts.

The variational problem is defined for numerical computation using a finite-element formulation provided by the FREEFEM++ library.[34] Discretization within the finite-element formulation is done via a (homogeneous) triangulation over Ω, based on the Delaunay-Voronoi algorithm. Functions are decomposed on a continuous piecewise quadratic basis on each triangle. The accuracy of such a method is controlled through the number of triangles (we typically used $3\text{–}6 \times 10^4$), the order of expansion of the basis on each triangle (P2 elements being of second-order-polynomial basis on each triangle), and also the order of the quadrature formula for the integral on the triangles.

Once the problem is mathematically well defined, a numerical optimization algorithm is used to solve the variational nonlinear problem (i.e., to find the minima of $\mathcal{F}$). We used here a nonlinear conjugate gradient method. The algorithm is iterated until the relative variation of the norm of the gradient of the functional $\mathcal{F}$ with respect to all degrees of freedom is less than 1×10^{-6}.

1. Initial guess

The initial field configuration carrying N flux quanta is prepared by using an ansatz which imposes phase windings around spatially separated N vortex cores in each condensate:

$$\psi_1 = |\psi_1| e^{i\Theta}, \quad \psi_2 = |\psi_2| e^{i\Theta + i\Delta_{12}}, \quad \psi_3 = |\psi_3| e^{i\Theta + i\Delta_{13}},$$
$$|\psi_j| = u_j \prod_{i=1}^{N_v} \sqrt{\frac{1}{2}\left[1 + \tanh\left(\frac{4}{\xi_j}[\mathcal{R}_i(x,y) - \xi_j]\right)\right]},$$
$$\mathbf{A} = \frac{1}{e\mathcal{R}}(\sin\Theta, -\cos\Theta), \tag{B1}$$

where $j = 1,2,3$ and u_j is the ground-state value of each superfluid density. The parameter ξ_j gives the core size while Θ and $\mathcal{R}$ are

$$\Theta(x,y) = \sum_{i=1}^{N_v} \Theta_i(x,y),$$
$$\Theta_i(x,y) = \tan^{-1}\left(\frac{y - y_i}{x - x_i}\right),$$
$$\mathcal{R}(x,y) = \sum_{i=1}^{N_v} \mathcal{R}_i(x,y), \tag{B2}$$
$$\mathcal{R}_i(x,y) = \sqrt{(x - x_i)^2 + (y - y_i)^2}.$$

The initial position of a vortex is given by (x_i, y_i). The functions $\Delta_{ab} \equiv \varphi_b - \varphi_a$ can be used to initiate a domain wall, when the ground state exhibits $U(1) \times Z_2$ symmetry.

[1] H. Suhl, B. T. Matthias, and L. R. Walker, Phys. Rev. Lett. **3**, 552 (1959).
[2] V. A. Moskalenko, Phys. Met. Metallogr. **8**, 503 (1959).
[3] J. Nagamatsu, N. Nakagawa, T. Muranaka, Y. Zenitani, and J. Akimitsu, Nature (London) **410**, 63 (2001).
[4] X. X. Xi, Rep. Prog. Phys. **71**, 116501 (2008).
[5] A. J. Leggett, Prog. Theor. Phys. **36**, 901 (1966).
[6] S. Sharapov, V. Gusynin, and H. Beck, Eur. Phys. J. **30**, 45 (2002).
[7] G. Blumberg, A. Mialitsin, B. S. Dennis, M. V. Klein, N. D. Zhigadlo, and J. Karpinski, Phys. Rev. Lett. **99**, 227002 (2007).
[8] V. Moshchalkov, M. Menghini, T. Nishio, Q. H. Chen, A. V. Silhanek, V. H. Dao, L. F. Chibotaru, N. D. Zhigadlo, and J. Karpinski, Phys. Rev. Lett. **102**, 117001 (2009).
[9] E. Babaev and M. Speight, Phys. Rev. B **72**, 180502 (2005).
[10] E. Babaev, J. Carlström, and M. Speight, Phys. Rev. Lett. **105**, 067003 (2010).
[11] T. Nishio, V. H. Dao, Q. Chen, L. F. Chibotaru, K. Kadowaki, and V. V. Moshchalkov, Phys. Rev. B **81**, 020506 (2010).
[12] R. Geurts, M. V. Milošević, and F. M. Peeters, Phys. Rev. B **81**, 214514 (2010).
[13] J. Carlström, J. Garaud, and E. Babaev, e-print arXiv:1101.4599, Phys. Rev. B in print.
[14] M. Silaev and E. Babaev, Phys. Rev. B **84**, 094515 (2011).
[15] V. H. Dao, L. F. Chibotaru, T. Nishio, and V. V. Moshchalkov, Phys. Rev. B **83**, 020503 (2011).
[16] J. Carlström, E. Babaev, and M. Speight, Phys. Rev. B **83**, 174509 (2011).
[17] Y. Kamihara, T. Watanabe, M. Hirano, and H. Hosono, J. Am. Chem. Soc. **130**, 3296 (2008).
[18] e. a. E. P. C. W. Chu, Physica C **469**, 313 (2009).
[19] P. J. Hirschfeld, M. M. Korshunov, and I. I. Mazin, e-print arXiv:1106.3712 (unpublished).
[20] T. K. Ng and N. Nagaosa, Europhys. Lett. **87**, 17003 (2009).
[21] V. Stanev and Z. Tešanović, Phys. Rev. B **81**, 134522 (2010).
[22] Y. Tanaka and T. Yanagisawa, Solid State Commun. **150**, 1980 (2010).
[23] X. Hu and Z. Wang, e-print arXiv:1103.0123 (unpublished).
[24] D. F. Agterberg, V. Barzykin, and L. P. Gor'kov, Phys. Rev. B **60**, 14868 (1999).
[25] W.-C. Lee, S.-C. Zhang, and C. Wu, Phys. Rev. Lett. **102**, 217002 (2009).
[26] C. Platt, R. Thomale, C. Honerkamp, S.-C. Zhang, and W. Hanke, e-print arXiv:1106.5964 (unpublished).
[27] S.-Z. Lin and X. Hu, e-print arXiv:1107.0814 (unpublished).

[28] Y. Ota, M. Machida, T. Koyama, and H. Aoki, Phys. Rev. B **83**, 060507 (2011).
[29] F. J. Burnell, J. Hu, M. M. Parish, and B. A. Bernevig, Phys. Rev. B **82**, 144506 (2010).
[30] A. Gurevich, Physica C **456**, 160 (2007).
[31] J. Smiseth, E. Smørgrav, E. Babaev, and A. Sudbø, Phys. Rev. B **71**, 214509 (2005).
[32] J. Garaud, J. Carlstrom, and E. Babaev, e-print arXiv:1107.0995 (unpublished).
[33] E. Babaev, Phys. Rev. Lett. **89**, 067001 (2002).
[34] F. Hecht, O. Pironneau, A. Le Hyaric, and K. Ohtsuka, FREEFEM++ *(manual)* (2007), [http://www.freefem.org].
[35] L. J. Li, T. Nishio, Z. A. Xu, and V. V. Moshchalkov, Phys. Rev. B **83**, 224522 (2011).
[36] M. R. Eskildsen, L. Y. Vinnikov, T. D. Blasius, I. S. Veshchunov, T. M. Artemova, J. M. Densmore, C. D. Dewhurst, N. Ni, A. Kreyssig, S. L. Bud'ko, P. C. Canfield, and A. I. Goldman, Phys. Rev. B **79**, 100501 (2009).
[37] M. Eskildsen, L. Vinnikov, I. Veshchunov, T. Artemova, T. Blasius, J. Densmore, C. Dewhurst, N. Ni, A. Kreyssig, S. Bud'ko, P. C. Canfield, and A. I. Goldman, Phys. C (Amsterdam) **469**, 529 (2009).
[38] Y. Yin, M. Zech, T. L. Williams, X. F. Wang, G. Wu, X. H. Chen, and J. E. Hoffman, Phys. Rev. Lett. **102**, 097002 (2009).
[39] L. Luan, O. M. Auslaender, T. M. Lippman, C. W. Hicks, B. Kalisky, J.-H. Chu, J. G. Analytis, I. R. Fisher, J. R. Kirtley, and K. A. Moler, Phys. Rev. B **81**, 100501 (2010).
[40] B. Kalisky, J. R. Kirtley, J. G. Analytis, J.-H. Chu, I. R. Fisher, and K. A. Moler, Phys. Rev. B **83**, 064511 (2011).